

# *In vitro* cytotoxic and genotoxic effects of *Phyllanthus niruri* extract loaded chitosan nanoparticles in TM4 cells and their influence on spermatogenesis

Ebrahim Sadaqa<sup>1</sup>, Ratna Annisa Utami<sup>1</sup>, Diky Mudhakir<sup>1</sup>

<sup>1</sup> Department of Pharmaceutics, School of Pharmacy, Institut Teknologi Bandung (ITB), Bandung, Indonesia

Corresponding author: Diky Mudhakir ([mudhakir@itb.ac.id](mailto:mudhakir@itb.ac.id))

Received 8 September 2023 ♦ Accepted 11 March 2024 ♦ Published 9 April 2024

**Citation:** Sadaqa E, Utami RA, Mudhakir D (2024) *In vitro* cytotoxic and genotoxic effects of *Phyllanthus niruri* extract loaded chitosan nanoparticles in TM4 cells and their influence on spermatogenesis. Pharmacia 71: 1–14. <https://doi.org/10.3897/pharmacia.71.e112138>

## Abstract

**Purpose:** This paper introduces a complete *in vitro* investigation of cytotoxic and genotoxic effects of *Phyllanthus niruri* extract loaded chitosan nanoparticles (PNNP) on mouse Sertoli cell line (TM4), as well as their impact on spermatogenesis.

**Methods:** Chitosan nanoparticles (ChNP) and PNNP were prepared using an ionic gelation process, while their cytotoxicity on TM4 cells was assessed using the Cell Counting Kit-8 (CCK-8) assay. Comet and fast halo assays were used to quantify single-strand DNA breaks in TM4 cells. To detect changes in cell morphology during apoptosis, nuclear staining with Hoechst 33342 was performed. An immunofluorescence assay was employed to examine the expression level of proteins connexin 43 and Claudin 11 in TM4 cells after exposure to PNNP concentration of 125 µg/mL.

**Results:** The synthesized PNNP had a size of 170.6 nm, a polydispersity index of 0.269, a zeta potential of +37.8 mV, and a good entrapment efficiency of 71.0%. Encapsulation of *Phyllanthus niruri* into ChNP induced DNA damage in TM4 cells as determined by alkaline comet and fast halo assay (FHA). Additionally, it stimulated apoptosis, as determined by changes in cell morphology by Hoechst 33342 staining. There was significant down regulation of blood-testis barrier (BTB) proteins in TM4 cells after exposure to PNNP which could compromise the integrity of BTB and subsequently disrupt spermatogenesis process in male.

**Conclusion:** Our investigation confirms the cytotoxic and genotoxic effects of PNNP in TM4 cells, which could lead to spermatogenesis disruption and male infertility.

## Keywords

Nanotoxicity, genotoxicity, *Phyllanthus niruri*, sertoli cell, DNA damage, immunofluorescence, BTB, spermatogenesis

## Introduction

*Phyllanthus niruri* has been the subject of extensive investigation in the field of pharmaceutical research (Kaur et al. 2017). This herbal medicine is composed of a diverse

array of bioactive compounds, including flavonoids such as quercetin, rutin, astragaloside, and niruriflavone, as well as lignans, terpenes, sterols, and polyphenols (Bagalkotkar et al. 2010). Due to the considerable content of quercetin flavonoids and their associated bioactivities, quercetin is

employed as a reference standard for evaluating the efficiency of extract entrapment (Pratiwi et al. 2019). A key pharmacological use that has been explored is the hepatoprotective capacity of *Phyllanthus niruri* to protect liver function and health (Ezzat et al. 2020). Spray-dried extract of *Phyllanthus niruri* has also been beneficial against acute colitis, reducing mucosal damage and inflammation through its antioxidant effects (De Melo et al. 2015). Beyond hepatic and gastrointestinal effects, emerging research suggests that *Phyllanthus niruri* has beneficial impacts on kidney function as well. Studies have indicated its ability to positively impact kidney function, suggesting its promise as a treatment for various kidney problems, including kidney stone prevention and enhancement of kidney cell proliferation (Freitas et al. 2002; Giribabu et al. 2017). However, excessive dosages or long-term use of *Phyllanthus niruri* may be harmful, as subsequent studies have investigated its toxicity on male reproductive function, producing hormonal imbalances and possible testicular degradation, which may lead to male infertility (Asare et al. 2013). Recently, nanoscale technology has proven an effective tool in boosting the therapeutic potential of medicinal plants. Drug delivery systems that employ *Phyllanthus niruri* nanoparticles hold great promise, including extract-loaded chitosan nanoparticles, which possess antibacterial effects against *Salmonella pullorum* (Hidanah et al. 2022). Additionally, *Phyllanthus niruri* nanoparticles are a promising candidate for prostate cancer therapy (Unni et al. 2014). Furthermore, *Phyllanthus niruri* extract nanoemulsion has antioxidant and antimicrobial activity (Pathania et al. 2022).

One area of research regarding *Phyllanthus niruri* that has attracted considerable interest is its extract in nanoparticle drug delivery systems, specifically for nanoparticles composed of chitosan, which have been found to possess immunomodulatory activity (Pratiwi et al. 2019). Chitosan is a natural polysaccharide linear with hydrophilic and cationic properties (Rizeq et al. 2019). Chitosan has long been known for being non-toxic and biodegradable by certain enzymes into non-toxic oligosaccharides, making it suitable for clinical applications as one of the most popular polymers for nanoparticles (Dash et al. 2011). However, when chitosan is synthesized as nanoparticles, its physicochemical properties change, and the nanoparticles may aggregate in a specific tissue via circulation, promoting harmful interactions between the nanoparticles and the human system (Loh et al. 2010). Nanoparticles easily penetrate cells with their large surface area and small size, and if positively charged or modified in other ways, they may enhance cell uptake (Hu and Gao 2010). Recent years have witnessed an increased focus on nanotoxicity research. Inorganic nanoparticles like silver nanoparticles, gold nanoparticles, metal oxide nanoparticles, and multi-walled carbon nanotubes, among others, have gained considerable interest within nanotoxicity research circles (Nagai et al. 2011; Puzyn et al. 2011; Yang et al. 2014). Nevertheless, there is still a dearth of information on the toxicity of organic nanoparticles. Recent research has found that sublethal doses of inorganic ZnO nanoparti-

cles caused reactive oxygen species (ROS) to be produced that interfered with Sertoli cells by reducing the expression of BTB protein. This suggests that ZnO nanoparticles could have toxic effects on male reproductive health (Liu et al. 2016). The potential toxicity of organic, biodegradable chitosan nanoparticles is not entirely known. According to a particular study, chitosan-based nanoparticles are less cytotoxic than free chitosan, supporting the belief that these nanoparticles are harmless (Frigaard et al. 2022). On the other hand, previous studies have demonstrated that chitosan nanoparticles may induce cellular apoptosis, the production of reactive oxygen species, and organ-specific damage in zebrafish models (Hu et al. 2011; Wang et al. 2016; Abou-Saleh et al. 2019). Therefore, assessing the potential toxicity of organic nanoparticles containing *Phyllanthus niruri*-loaded chitosan nanoparticles (PNNP) is crucial to ensure their safe clinical application.

At the core of this research lies an inquiry into the impact of PNNP on Sertoli cells, which play an essential role in spermatogenesis. We aim to explore any cytotoxic or genotoxic effects PNNP may have using the TM4 cell line and evaluate toxicity levels from these nanoparticles and their carrier nanoparticles (ChNP) concerning their impact on spermatogenesis. Given their possible adverse effects on male reproductive health, thorough investigations of toxicities must be conducted before widespread usage in clinical settings.

## Materials and methods

### Materials

Sodium tripolyphosphate (STPP), quercetin, bovine serum albumin (BSA), normal melting point agarose (NMA), triton X-100, ethidium bromide and Cell counting kit -8 (CCK-8) were purchased from Sigma-Aldrich (St. Louis, MO). Chitosan was purchased from PT. Biotech Surindo (Cirebon, Indonesia). Dry extract of *Phyllanthus niruri* (meniran) was purchased from PT. Borobudur Extraction Center (Semarang, Indonesia). Absolute ethanol, glacial acetic acid, sodium hydroxide, methanol pro-analysis, aluminium chloride, sodium acetate, sodium chloride, dimethyl sulfoxide, disodium ethylenediaminetetraacetic acid (EDTA) were purchased from Merck (Rahway, NJ). Phosphate buffer saline (PBS), dulbecco's modified eagle medium (DMEM high glucose), F12 nutrients, fetal bovine serum (FBS), penicillin-streptomycin were purchased from Gibco, Thermo Fisher Scientific (Waltham, MA). Trypan blue, 0.25% trypsin solution and trypsin-EDTA solution were purchased from Invitrogen (Carlsbad, CA). Low melting point agarose (LMA) was purchased from Himedia Laboratories (Maharashtra, India). TM4 cell was supplied by European Collection of Authenticated Cell Cultures (ECACC) Catalogue no. 88111401 (Salisbury, UK). Primary polyclonal antibodies of claudin 11 and connexin 43, and secondary antibody of goat anti-rabbit IgG (H+L) cross-adsorbed, Alexa Fluor 488 were purchased from Thermo Fisher Scientific (Waltham, MA).

## Preparation of empty ChNP and PNNP

The ionic gelation process was used to prepare PNNP. A chitosan solution with a concentration of 1.4 mg/mL was prepared in 1% v/v glacial acetic acid. The pH was adjusted to 4.7 using 5 M NaOH, and the solution was filtered using a 0.22 µm Techno Plastic Products (TPP) syringe filter. STPP solution was prepared in deionized water with a concentration of 1.47 mg/mL to be used as a crosslinker and then filtered using a 0.22 µm TPP syringe filter. The stock solution of *Phyllanthus niruri* extract was produced at a concentration of 5000 µg/mL, then filtered through a 0.22 µm TPP syringe filter, and the concentration of extract used in each final formula was 2500 µg/mL. The *Phyllanthus niruri* nanoparticles formulation method began with adding 50 µL of previously made *Phyllanthus niruri* extract to 712 µL chitosan solution in a brown glass vial. Furthermore, as described, this addition was repeated in 10 brown glass vials (total volume of *Phyllanthus niruri* extract that was added 500 µL and chitosan solution 7120 µL) and incubated for 30 min in a darkroom. Then, each glass vial containing *Phyllanthus niruri* extract and chitosan solution was stirred using a magnetic stirrer at 800 rpm for 1 min, after which 238 µL of STPP solution was titrated using a micropipette drop by drop, stirring was continued for 2 min. After adding STPP, nanoparticles will form immediately. Each glass vial component (1000 µL) was aspirated into a 1.5 mL microcentrifuge tube, then centrifuged at 13000 rpm for 20 min. The supernatant was collected for a subsequent entrapment efficiency test. Each pellet was resuspended in 100 µL of deionized water and collected in one clean glass vial with a total volume of 1000 µL. Sonication was carried out for the final solution of nanoparticles (1000 µL) with an amplitude of 70% for 10 seconds three times. In the preparation of ChNP, the same steps as before were followed with just some slight modifications; only distilled water was used instead of *Phyllanthus niruri* extract.

## Physical characterization of ChNP and PNNP

Determination of particle size, polydispersity index (PDI), and zeta potential was measured using Photon Correlation Spectroscopy with the working principle of the tool analyzing fluctuations in light scattering using the Delsa Nano C Particle Size Analyzer (Beckman Coulter).

## Entrapment efficiency (EE) of PNNP

The EE of PNNP was determined using an indirect method. The unencapsulated drug was quantified by measuring the total flavonoid content in the supernatant solution collected from the nanoparticles during formulation after centrifugation. The content analysis was conducted using the total flavonoid test for *Phyllanthus niruri* extract, and quercetin was used as a standard comparison compound as stated in the Indonesian Herbal Pharmacopoeia (Kemenkes 2017). A stock solution of 1000 ppm quercetin in methanol was prepared, and a calibration curve was created at concentrations of 30, 40, 50, 60, 70, 80, and 90 ppm. The calibration curve was generated by mixing 0.5 mL of standard with 0.1 mL AlCl<sub>3</sub> 10%, 0.1 mL NaAcetate 1 M, 1.5 mL methanol, and 2.8 mL demineralized water. The spiked sample was prepared by adding 0.5 mL of the sample with 0.5 mL of spiked standard quercetin, 0.1 mL AlCl<sub>3</sub> 10%, 0.1 mL Na Acetate 1M, 1.5 mL methanol, and 2.3 mL demineralized water. The blank sample was prepared by mixing 1.5 mL of methanol, 0.1 mL of 1M sodium acetate, and 3.4 mL of demineralized water. The samples were then incubated in a dark room for 30 minutes. The concentration of quercetin was quantified using a UV-visible spectrophotometer (T92+ Spectrophotometer Pg instruments) at 434 nm. These steps were repeated three times. The EE of the nanoparticles was calculated using the formula below:

$$\%EE = \frac{\text{Total flavonoid content of extract } 250 \text{ ppm} - \text{total flavonoid content of supernatant}}{\text{Total flavonoid content of extract } 250 \text{ ppm}} \times 100$$

## Morphology investigation

The morphology of formulated ChNP and PNNP were examined by transmission electron microscopy (TEM) imaging. TEM analysis was performed using a Hitachi HT7700 TEM system (Tokyo, Japan). For sample preparation, the nanoparticle solutions were diluted with deionized water, then pipetted directly onto carbon-coated copper grids prior to TEM imaging. The TEM analysis enabled assessment of the particle size distribution and morphological characterization of both the ChNP and PNNP formulations (Mohamed et al. 2023).

## Fourier transform infrared (FTIR) spectroscopy

FTIR spectroscopy was performed to analyze the chemical composition and structure of the nanoparticles. FTIR

spectra were obtained using a Jasco FT/IR-4200 type A spectrometer equipped with an attenuated total reflectance (ATR) accessory. A small amount of each sample (*Phyllanthus niruri* (PN) extract, chitosan powder, sodium tripolyphosphate (STPP) crosslinker, and PNNP) was placed on the ATR crystal and a single reflection spectrum was collected over the range of 4000–400 cm<sup>-1</sup> with a resolution of 16 cm<sup>-1</sup>. Each spectrum represented an average of 16 scans. The spectra were compared to analyze changes in functional groups and molecular structure after nanoparticle formation.

## Thermal analysis

Thermal analysis was conducted using a STA 7300 simultaneous thermal analyzer (Hitachi High-Tech Science Corporation, Japan). Samples weighing 0.592 mg of ChNP and

0.592 mg of PNNP were separately placed into platinum crucibles and subjected to heating from 25 °C to 800 °C at a rate of 10 °C/min under a 30 mL/min nitrogen atmosphere. An empty aluminum oxide (Al<sub>2</sub>O<sub>3</sub>) crucible served as the reference. The STA 7300 analyzer facilitated comprehensive analysis, detecting transitions including glass transitions, crystallization, oxidation, and decomposition events. Differential thermal analysis (DTA) produced a plot of heat flow signal against temperature, while thermogravimetric analysis (TGA) displayed a percentage sample weight change against temperature. Additionally, Differential Thermogravimetric Analysis (DTG) enabled the observation of the rate of change of weight loss against temperature, offering insights into specific thermal events (Ramos et al. 2023).

### Cell viability test using CCK-8 assay

To investigate the cell viability of nanoparticles,  $5 \times 10^3$  TM4 cells were seeded on 96-well plates in 100 µL of DMEM medium containing 10% FBS, 100 U/mL penicillin and 100 µg/mL streptomycin and incubated for 24 h. Two types of nanoparticles: ChNP and PNNP were exposed to the cells and incubated for another 24 h. Series concentration of *Phyllanthus niruri* in PNNP was 7.8, 31.3, 125, 500, and 2000 µg/mL, respectively. Meanwhile, the concentration of ChNP was prepared corresponding to concentration dilutions of PNNP. Untreated cells served as the negative control and cells treated with 5% Tween 20 as the positive control. After adding 10 µL of CCK-8 solution to each well, the plates were incubated at 37 °C for 1 h and the absorbance was measured at 450 nm using a microplate reader. The experiments were performed in triplicate and the results were expressed as mean  $\pm$  SD. The inhibitory concentration (IC50) was calculated using CompuSyn software.

### Quantification DNA damage by alkaline comet assay

The alkaline comet assay was conducted based on the previously described method (Dusinska et al. 2017). Briefly, TM4 cells were seeded at a density of  $3.0 \times 10^5$  in a multi-well plate and incubated at 37 °C in a 5% CO<sub>2</sub> atmosphere for 24 h. Then, cells were treated independently with two groups of tested medications: ChNP at concentrations of 25, 50, and 200 µg/mL, and PNNP at concentrations of 62.5, 125, and 500 µg/mL. The treatment duration was 2 h. The negative control was untreated cells while the positive control was cells incubated with H<sub>2</sub>O<sub>2</sub> (100 µM) for 15 min. Each experiment was repeated three times. After treatment, cells were harvested into 15 mL tubes by aspirating the medium, washing with PBS (calcium- and magnesium-free), adding trypsin, collecting in a tube, and neutralizing trypsin with appropriate serum-containing media. Cells were then centrifuged in tubes at 200 g for 7 min; the medium was discarded, and cell pellets were resuspended in PBS. All cells were collected under dim light conditions. About 75 mg of LMA was placed in a conical flask with 10 mL of PBS and heated in a microwave until

the agarose dissolved completely and the mixture became transparent. The mixture was transferred to eppendorf tubes and kept in a water bath at 37 °C until needed. After cell collection, 30 µL of cell suspension ( $3 \times 10^4$  cells) and 90 µL of LMA solution (0.75%) at 37 °C (1:4 ratio) were mixed well with a pipette, and 60 µL of the mixture was quickly added to each side of the pre-coated NMA slide to create two gel layers. The slides were covered rapidly with coverslips and placed in the fridge for 5 min until the gel solidified. The coverslip was then carefully removed, and the slides were submerged in a coplin jar covered with aluminum foil containing freshly prepared lysis buffer (2.5 mM NaCl, 100 mM EDTA, and 10 mM Tris HCl) adjusted to pH 10. This solution was supplemented with 10% DMSO and 1% Triton X-100, 30 minutes prior to the commencement of the experiment. The slides were left in the lysing buffer overnight at 2–4 °C. Following lysis, the slides were placed horizontally in electrophoresis buffer (0.3 M NaOH and 1 mM EDTA) for 30 minutes to unwind the DNA. Electrophoresis was then performed for 30 minutes at 4 °C at 300 mA and 25 volts. The slides were subsequently submerged in neutralization buffer (0.4 M Tris-HCl, pH 7.5) for 5 minutes at 4 °C in a dark place, followed by 5 minutes in cold distilled water. The DNA was visualized in a dark room by staining the slides with 60 µL of ethidium bromide (20 µg/mL). The slides were covered with a coverslip and scored after 10 minutes to avoid cell dehydration. The DNA integrity of 50–100 cells per slide was randomly scored using an Inverted Microscope Olympus IX73 filter connected to the CCD. The data were transferred to another computer and analyzed using CASP software. Olive tail moment (OTM) is the more frequently used to measure DNA damage. However, providing in parallel with % tail DNA is recommended (Tice et al. 2000). Thus, two parameters, % tail DNA (the percentage of DNA in the tail) and OTM (fraction of DNA in the tail multiplied by the tail length), were used to assess DNA damage in the comet assay.

### Assessment of DNA single strand breaks (SSBs) by FHA

DNA SSBs were detected using the FHA method as previously described (Sestili et al. 2006), with the following modification. TM4 cells were seeded at a density of  $4.0 \times 10^5$  cells and incubated in a 5% CO<sub>2</sub> atmosphere at 37 °C for 24 h. After incubation, the cells were treated with various doses of ChNP and PNNP medications. The incubation duration was 2 h. The negative control consisted of untreated cells, while the positive control involved incubating cells with 100 µM of H<sub>2</sub>O<sub>2</sub> for 15 min. After treatment, cells were collected under dim light, and the supernatant was discarded. Cells were washed with ice-cold PBS containing 5 mM EDTA and then resuspended at  $4.0 \times 10^4$  cells/100 µL ice-cold PBS containing 5 mM EDTA. The cell suspension was diluted with an equal volume of 2% LMA in PBS, which was kept in a water bath at a temperature of around 37 °C. Sixty microliters of the

mixture was immediately pipetted onto precoated slides with 1% NMA and covered with a coverslip. The slides were then placed on an aluminum foil and put on ice for about 20 min until the agarose layers hardened. The coverslips were gently removed, and the slides were placed in a coplin staining jar with 300 mM NaOH to cover the slides and incubated in a dark place for 15 min. In the last 5 min of incubation, ethidium bromide (10 µg/mL) was added, and the slides were destained with distilled water for 5 min. The slides were immediately examined under an inverted microscope Olympus IX73. The DNA integrity of 50 cells per slide was scored, and the level of DNA breakage in each scored cell was expressed by the Nuclear Diffusion Factor (NDF). NDF values of 50 randomly selected cells were calculated semi-automatically on each slide using HaloJ (Maurya 2014). Each experiment was repeated three times, and values are presented as the mean  $\pm$  standard error of the mean (SEM). All data were analyzed using one-way ANOVA followed by Kruskal-Wallis for multiple comparisons using the Graph-Pad Prism 8 software. The stars indicate a significant difference between control negative (untreated cells) and various treatment groups ( $P < 0.05$  significantly different). The data with a  $p$ -value  $\geq 0.05$  was determined as nonsignificant (ns). A  $p$ -value score of between 0.01 and 0.05 was determined as significant (\*), between 0.01 and 0.001 as very significant (\*\*), and  $< 0.001$  as extremely significant (\*\*\*)

### Investigation of cellular morphological change by Hoechst 33342 nuclear staining

Hoechst 33342 is a blue-fluorescence DNA-specific dye that stains the condensed chromatin in apoptotic cells (Schmid et al. 2007). Apoptotic cells exhibit nuclear condensation and DNA fragmentation, which can be detected with a fluorescence microscope and the dye Hoechst 33342 (Allen et al. 2001). To assess cellular morphological changes during apoptosis qualitatively, we employed Hoechst 33342 staining. In brief, TM4 cells were seeded into a 35-mm glass-base dish at a density of  $5 \times 10^4$  cells per plate and cultured at 37 °C. When the cells reached 70–80% confluency, they were treated with PNNP at a concentration of 125 µg/mL, ChNP at concentrations of 50 and 200 µg/mL, which were dilutions equivalent to PNNP at 125 and 500 µg/mL, respectively. After 2 h of incubation at 37 °C, the medium was aspirated and the plates were rinsed with PBS, fixed with 4% PFA for 15 min, washed with PBS for 5 min, then stained with 1 µg/mL Hoechst 33342 at 37 °C for 15 min in a dark place. Following that, the cells were rinsed with PBS and examined under Confocal Laser Scanning Microscope (Olympus FV-1200).

### BTB proteins expression using immunofluorescence assay

The goal of the immunofluorescence test in this study is to assess the influence of PNNP and ChNP on connexin 43

and claudin 11 protein expression in TM4 cells. In brief, TM4 cells were seeded into a 35-mm glass-base dish at a density of  $1 \times 10^5$  cells in 2 mL of DMEM containing 10% FBS and incubated in an atmosphere of 5% CO<sub>2</sub> at 37 °C for 24 h. The cells were then treated with PNNP or ChNP independently. In this study, concentration of PNNP used was 125 µg/mL, while that for the ChNP was 50 and 200 µg/mL, which were dilutions equivalent to PNNP at 125 and 500 µg/mL, respectively. Additional cells were also left untreated to serve as a control. The cells were incubated for 24 h at 37 °C in the presence and absence of nanoparticles. The media was aspirated, and the cells were washed twice with 1 mL of PBS. The cells were fixed in 4% formaldehyde for 15 min at room temperature. The cells were then rinsed three times with 1 mL of ice-cold PBS for 5 min. The cells were incubated in 1 mL of permeabilization buffer, PBST (0.1% Triton X-100 in PBS), for 10 min at room temperature, followed by washing steps three times with 1 mL of PBS. Unspecific sites were blocked in a blocking buffer containing 5% BSA in PBS for an hour at room temperature, followed by the washing steps. Cells were incubated with primary antibody (with a concentration of 4 µg/mL diluted in blocking buffer) overnight at 4 °C and then washed with PBS three times for 5 min each. Cells were then incubated with a secondary antibody (with a concentration of 4 µg/mL diluted in blocking buffer) in the dark at room temperature for an hour, followed by washing steps. Cells were stained with Hoechst 33342 (1 µg/mL) for 10 min in the dark, followed by mounting medium, and coverslips were placed on top and examined under Confocal Laser Scanning Microscope (Olympus FV-1200).

## Results and discussion

### Physicochemical characterization of nanoparticles

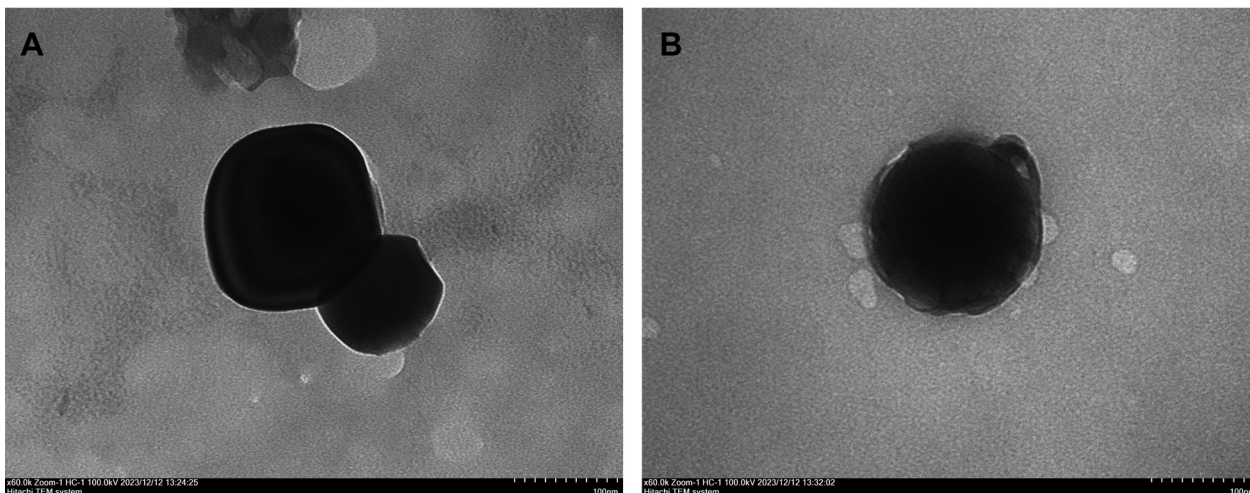
ChNP were successfully synthesized at a concentration of 997 µg/mL of chitosan, with a mean droplet size of  $169.46 \pm 7.46$  nm, a mean PDI of  $0.269 \pm 0.026$  as shown in Table 1. PNNP were also successfully formulated at a 2500 µg/mL concentration, with a mean droplet size of  $170.69 \pm 6.32$  nm and a mean PDI of  $0.269 \pm 0.026$ . The polydispersity index (PDI) is an indicator of homogeneity. In this study, PDI values of all formulations were less than 0.5, indicating more monodisperse systems considerably with minimal variability and no aggregation (Mahmood et al. 2019). The results of the zeta potential and entrapment efficiency have been presented in Table 1. The mean zeta potential of ChNP ( $38.77 \pm 1.81$  mV) and PNNP ( $37.82 \pm 1.91$  mV) indicated that the resulting nanoparticles had sufficient electrostatic repulsion to maintain colloidal stability. The entrapment efficiency was calculated indirectly, using the total flavonoid content. A calibration curve was established using standard quercetin at a wavelength of 434 nm, with the equation  $y = 0.0087x + 0.0047$  ( $R^2 = 0.998$ ). The entrapment efficiency value of PNNP in this study was found to be  $71.41\% \pm 3.79$ .

**Table 1.** Physicochemical characterization of ChNP and PNNP (n = 3).

Groups	Mean droplet particle size (nm)	Mean polydispersity index (PDI)	Mean Zeta Potential (mV)	Entrapment Efficiency (%)
ChNP	169.46 ± 7.46	0.293 ± 0.066	38.77 ± 1.81	NA
PNNP	170.69 ± 6.32	0.269 ± 0.026	37.82 ± 1.91	74.45%

## Morphology investigation

The ChNP in Fig. 1A display a smooth, spherical morphology with no visible surface indentations or irregularities, confirming the uniform chitosan polymer matrix that forms these nanoparticles. In comparison, the PNNP in Fig. 1B show a rough surface morphology, with visible protuberances, cavities and some loss of a smooth outline caused by the incorporation of the *Phyllanthus niruri* components into the nanoparticle matrix.

**Figure 1.** Transmission electron microscope (TEM) images showing morphology of **A.** unloaded ChNP compared to **B.** PNNP. The scale bar represents 100 nm.

## Fourier transform infrared spectroscopy (FTIR)

The FTIR spectra of PN extract, chitosan powder, STPP crosslinker and PNNP, are displayed in Fig. 2. The FTIR spectrum of PN extract revealed distinctive peaks denoting aromatic rings ( $1563\text{ cm}^{-1}$ ) and carbonyl groups ( $1641\text{ cm}^{-1}$ ). Additionally, a broad peak present of around  $3395\text{ cm}^{-1}$  can be ascribed to the O–H stretching vibrations of alcohols, phenols, or carboxylic acids. The peak at  $2922\text{ cm}^{-1}$  corresponds to the C–H stretching vibrations of aliphatic groups.

The spectrum of chitosan powder exhibits characteristic peaks at  $1654\text{ cm}^{-1}$  indicating N–H bending suggests the presence of amines, and a broad band at  $3423\text{ cm}^{-1}$  attributed to the overlapping O–H and N–H stretching vibrations, consistent with its structure (Kahdestani et al. 2021; Vaezifar et al. 2013). The STPP crosslinker agent displayed characteristic phosphate bands around  $890\text{--}1200\text{ cm}^{-1}$ .

The FTIR spectrum of PNNP exhibited the confluence of peaks stemming from PN extract, chitosan, and STPP. The broad peak at approximately  $3395\text{ cm}^{-1}$  can be ascribed to the O–H stretching vibrations of hydroxyl and carboxylic acid groups originating from PN extract, as well as the O–H and N–H stretching vibrations of hydroxyl and amine groups stemming from chitosan. The peak situated at  $2922\text{ cm}^{-1}$  corresponds to the C–H stretching vibrations of aliphatic groups present in both PN extract and chitosan. The conceivable interactions between PN extract and chitosan may take the form of hydrogen bonding or electrostatic interactions between the hydroxyl and amine groups of chitosan and the functional groups of PN extract, such as carboxylic acids or phenols. Moreover, the interactions between STPP and chitosan can manifest as ionic bonding between the phosphate groups of STPP and the amine groups of chitosan. In essence, the FTIR results imply that the components of PNNP primarily engage in physical interactions.

## Thermal analysis

The thermal properties and stability of ChNP and PNNP were thoroughly examined using thermal analysis, as shown in Fig. 3. Fig. 3A displays the results for ChNP, while Fig. 3B shows the findings for PNNP. The thermogravimetric analysis (TGA) data clearly demonstrated differing thermal degradation patterns between ChNP and PNNP. PNNP showed rapid degradation within  $100\text{--}200\text{ }^{\circ}\text{C}$ , a trend less noticeable in ChNP. This indicates modified thermal stability of chitosan nanoparticles following the incorporation of *Phyllanthus niruri* extract, likely due to the extract's high volatile oil content, increasing susceptibility to lower temperature degradation (Moseson et al. 2020).

As the temperature was further increased to  $300\text{ }^{\circ}\text{C}$ , additional weight loss was observed. Remarkably, a steep weight reduction occurred in ChNP between  $300\text{--}500\text{ }^{\circ}\text{C}$ , consistent with previous studies (Daramola and Adelaja 2020). In contrast, PNNP exhibited a more gradual decline in weight across a wider  $200\text{--}500\text{ }^{\circ}\text{C}$  range.

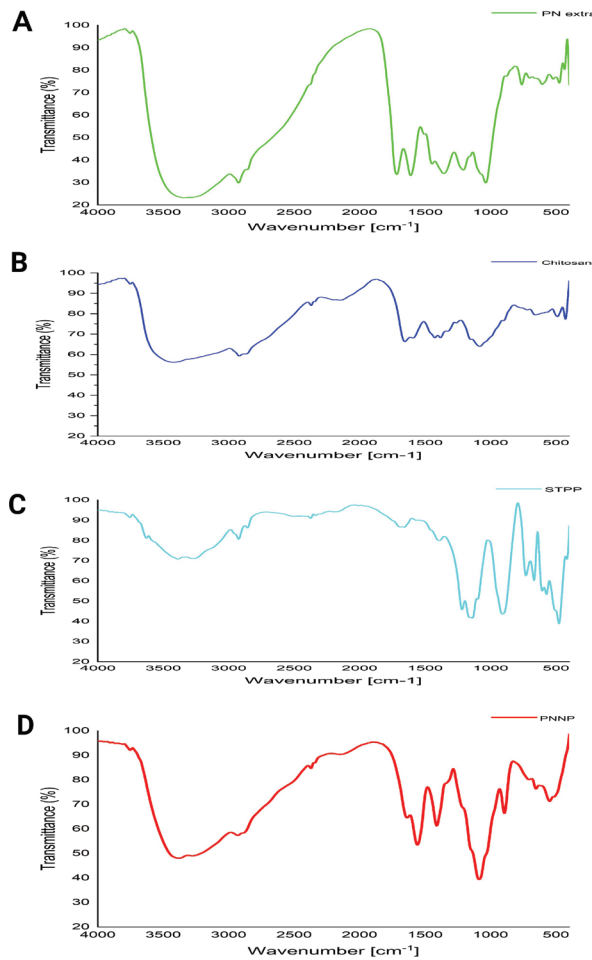


**Figure 2.** FTIR spectra of **A.** PN extract; **B.** chitosan; **C.** STPP; **D.** PNNP.

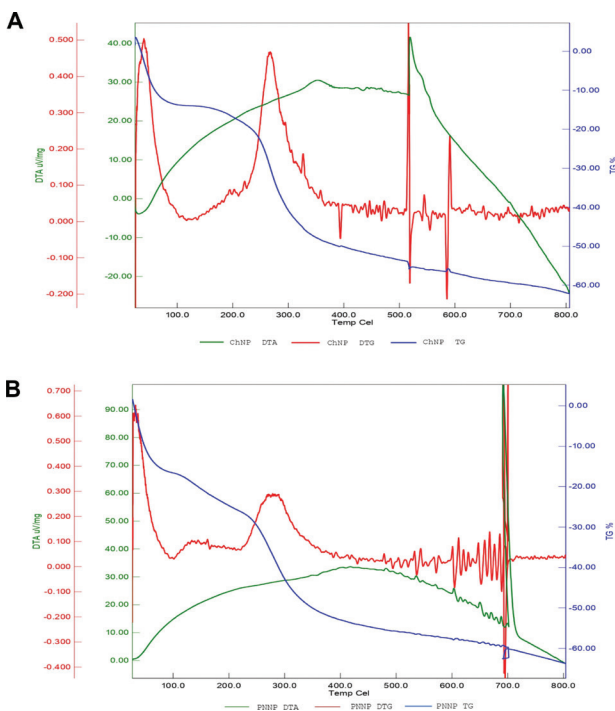


**Figure 3.** Illustration of the TGA, DTG, and DTA curves for **A.** ChNP and **B.** PNNP. DTA curves are represented in green, DTG curves in red, and TGA curves in blue.

The considerable weight loss from 300–500 °C for ChNP may be attributed to the degradation of the chitosan polymer backbone, aligning with literature documenting chitosan decomposition above 300 °C. Meanwhile, the gradual PNNP weight change over 200–500 °C could signify combined degradation of both chitosan nanoparticles and loaded *Phyllanthus niruri* component. Furthermore, differential thermogravimetry (DTG) analysis provided confirmation. A distinct peak near 150 °C appeared exclusively in PNNP, absent in ChNP, signifying *Phyllanthus niruri* degradation from the nanoparticles. At 300 °C, ChNP displayed a sharp DTG peak, contrasting the broader PNNP peak initiating at 250 °C. This proposes a wider temperature scope for PNNP thermal degradation, potentially owing to the extract's high flavonoid content, recognized to typically decompose above 250 °C (Sricharoenchaikul and Atong 2009). The broad peak may indicate combined degradation of chitosan nanoparticles and loaded *Phyllanthus niruri* components.

Differential thermal analysis (DTA) did not reveal distinct endothermic or exothermic peaks associated with melting or crystallization processes for either ChNP or PNNP. Nevertheless, the significant variations observed in TGA and DTG curves offer compelling evidence for the successful encapsulation of *Phyllanthus niruri* extract. These variations indicate a notable alteration in the thermal stability and decomposition behavior of the nanoparticles.

### Cell viability assay on ChNP and PNNP with CCK-8

The cytotoxicity studies on the TM4 cells were carried out after exposure to various concentrations of ChNP and PNNP for 24 h.

The results of cell viability (%) for TM4 cells treated with ChNP and PNNP are shown in Fig. 4, indicating that there was no significant cytotoxic effect observed when TM4 cells were treated with ChNP dilutions equivalent to those used for PNNP at concentrations of 7.8, 31.3, 125, 500, and 2000 µg/mL. These findings are consistent with recent research indicating a non-significant effect of ChNP on zebrafish embryo survival at concentrations of 25, 50, 100, and 200 mg/L, further supporting the non-cytotoxic nature of ChNP (Abou-Saleh et al. 2019). Conversely, cell viability was reduced when the cells were treated with PNNP and Tween-20. A significant difference was observed with p-values of  $^{**}p = 0.001$  in cells treated with PNNP at 7.8 µg/mL and  $^{***}p < 0.001$  in cells treated with PNNP at concentrations of 31.3, 125, 500, and 2000 µg/mL, as well as Tween-20 at a concentration of 5% as a positive control. The concentration at which PNNP decreased cell viability to 50% (IC<sub>50</sub>) was determined to be 451.24 µg/mL using CompuSyn software.

### Quantitative analysis of DNA damage by alkaline comet assay

The comet assay was employed to evaluate DNA damage in TM4 cells by calculating the OTM and percentage of tail DNA parameters (Wu and Jones 2012).

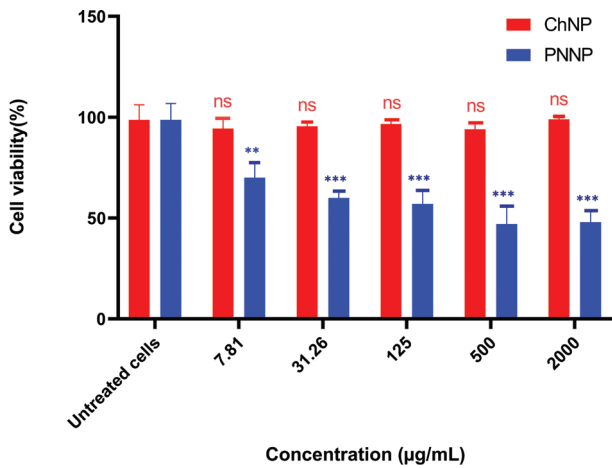


**Figure 4.** Cell viability percentage after 24 hours of exposure to various concentrations of ChNP and PNNP assessed by CCK8 test. The values are presented as mean  $\pm$  standard deviation (SD) ( $n = 3$ ). All data were analyzed using One-way ANOVA. The stars indicate significant difference between control negative (untreated cells) and various treatment groups ( $P < 0.05$  significantly different,  $p$ -value  $\geq 0.05$  was determined as non-significant (ns). A  $p$ -value score of between 0.01 and 0.05 was considered significant (\*), between 0.01 and 0.001 as very significant (\*\*), and  $< 0.001$  as extremely significant (\*\*\*)).

The results are presented in Fig. 5. When TM4 cells were treated with ChNP 25 and 50  $\mu\text{g}/\text{mL}$ , there was no comet formation of DNA as shown in Fig. 5c, d. In line with the

qualitative images data, semi-quantitative data of the OTM and % tail DNA also did not show any significant difference from the untreated cells. However, when the concentration of ChNP increased to 200  $\mu\text{g}/\text{mL}$ , nucleoid bodies indicating DNA damage that migrated away from undamaged DNA were detected to form comet (Fig. 5e). Additionally, the OTM and % tail DNA increased significantly of approximately 3 and 28% with a  $p$ -value  $***p < 0.001$ , respectively (Fig. 5i, j). These results imply that this concentration induced single-strand DNA breaks and DNA damage accumulated in TM4 cells. When *Phyllanthus niruri* was encapsulated into ChNP 25, 50 and 200  $\mu\text{g}/\text{mL}$  (correspond to PNNP 62.5, 125 and 500  $\mu\text{g}/\text{mL}$ , respectively), it exhibited that at higher concentrations of loaded *Phyllanthus niruri*, longer DNA tails were formed (Fig. 5f–h). These findings are consistent with an earlier report that showed chitosan-reduced gold nanoparticles demonstrated concentration-dependent DNA damage (Nandanpawar et al. 2018). In addition, reflecting the qualitative data of genotoxic ChNP, the OTM and % tail DNA were also gradually enhanced depending on the PNNP concentration which demonstrated a significant influence on DNA of TM4 cells with a  $p$ -value  $***p < 0.001$  (Fig. 5i, j). Based on our findings, it also can be inferred that the genotoxic effect of PNNP is primarily attributed to the specific *Phyllanthus niruri* extract used in its preparation at the nanoscale. This fact is supported by the results of PNNP 62.5 and 125  $\mu\text{g}/\text{mL}$  which had a significant genotoxic effect on cell DNA while their empty carriers (ChNP 25 and 50  $\mu\text{g}/\text{mL}$ ) did not induce the effect.

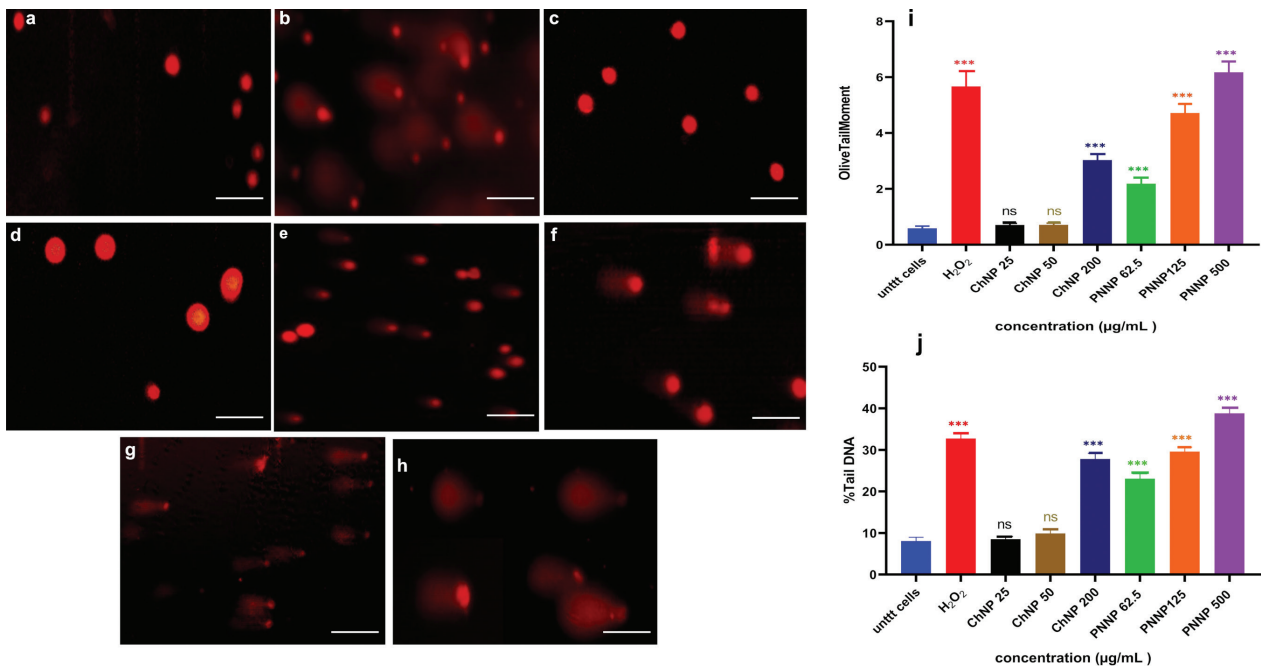


**Figure 5.** DNA damage caused by ChNP and PNNP using comet assay. TM4 cells were incubated with various concentrations of ChNP and PNNP for 2 h. Positive control 100  $\mu\text{M}$  H<sub>2</sub>O<sub>2</sub> was used and incubated for 15 min. Comet images demonstrating the degree of DNA damage on TM4 cells were captured using Inverted Microscope Olympus IX73. Single stranded DNA was stained with ethidium bromide. Comet images displayed untreated cells as control (a), H<sub>2</sub>O<sub>2</sub>-treated cells (b), and ChNP-treated cells at concentrations of 25  $\mu\text{g}/\text{mL}$  (c), 50  $\mu\text{g}/\text{mL}$  (d), and 200  $\mu\text{g}/\text{mL}$  (e), as well as PNNP-treated cells at concentrations of 62.5  $\mu\text{g}/\text{mL}$  (f), 125  $\mu\text{g}/\text{mL}$  (g), and 500  $\mu\text{g}/\text{mL}$  (h). The bar indicates 5  $\mu\text{m}$ . Quantitative assessment of DNA damage was performed by measuring olive tail moment (i) and % tail DNA (j). The data are presented as the mean  $\pm$  SEM of three independent trials ( $n=200$ ), ns (not significant) ( $***p < 0.001$ ,  $**p < 0.01$ ,  $*p < 0.05$  when compared to the corresponding control group).

These findings emphasize the need for caution when using *Phyllanthus niruri* extract at the nanoscale in the development of safe and effective therapeutic interventions.

Despite the fact that ChNP 200  $\mu\text{g}/\text{mL}$  demonstrated 94% cell survival, it significantly induced DNA damage in TM4 cells, as previously mentioned. Therefore, as recommended by several studies, it is crucial to investigate the genotoxicity of all new nanoparticles. Traditional *in vitro* toxicity testing has mainly focused on evaluating cytotoxicity assays to determine whether exposure to a potentially toxic substance, such as nanomaterials, leads to cell death or damage (Lewinski et al. 2008). However, exposure to nanomaterials may cause changes in cellular function, genomic disruption, or potential organ-specific toxicity, as demonstrated in previous research where ChNP exhibited a non-cytotoxic effect on zebrafish embryos but induced neurobehavioral toxicity and liver size impairment at high concentrations of 200 mg/L (Abou-Saleh et al. 2019). Hence, it is imperative to investigate other forms of toxicity, such as genotoxicity, to ensure the safety of using these nanoparticles in human health.

### Evaluation of DNA breakage by FHA

To assure the results by comet assay, we also assessed the extent of DNA damage in TM4 cells using the FHA. The

FHA presents some analogies with comet assay; however it is further simplified through excluding the high-salt lysis step in extraction of single-stranded (ss) DNA from agarose-embedded cells and extraction of ssDNA directly in alkaline buffer NaOH. Thus, this method is simpler and more rapid than the comet assay (Sestili et al. 2006). Halo images that referred to shape of radial diffusion of DNA fragments from isolated nuclei were then captured by fluorescence microscope. To allow analytical data of treatments on TM4 cells, DNA strand scission level was quantified by calculating the NDF which represents the ratio between the total area of the halo plus nucleus and that of the nucleus. As results, the use of ChNP 25 and 50  $\mu\text{g}/\text{mL}$  had no halo spreading observed so that there was no significant effect (ns) on DNA SSBs in TM4 cells compared to untreated cells (p-value > 0.05), as shown in Fig. 6c, d. However, the ChNP 200  $\mu\text{g}/\text{mL}$  exhibited the radial diffusion of DNA fragments significantly to that of the non-treatment (p-value \*\*\*p < 0.001) (Fig. 6e). It is worth noting that ChNP 200  $\mu\text{g}/\text{mL}$  exhibited 94% cell viability, however it also caused significant ssDNA damage in TM4 cells, suggesting potential genotoxicity as evaluated by comet assay and FHA. These findings indicate that caution should be exercised when using ChNP at this concentration. Subsequent studies should be conducted to further evaluate the safety of ChNP.

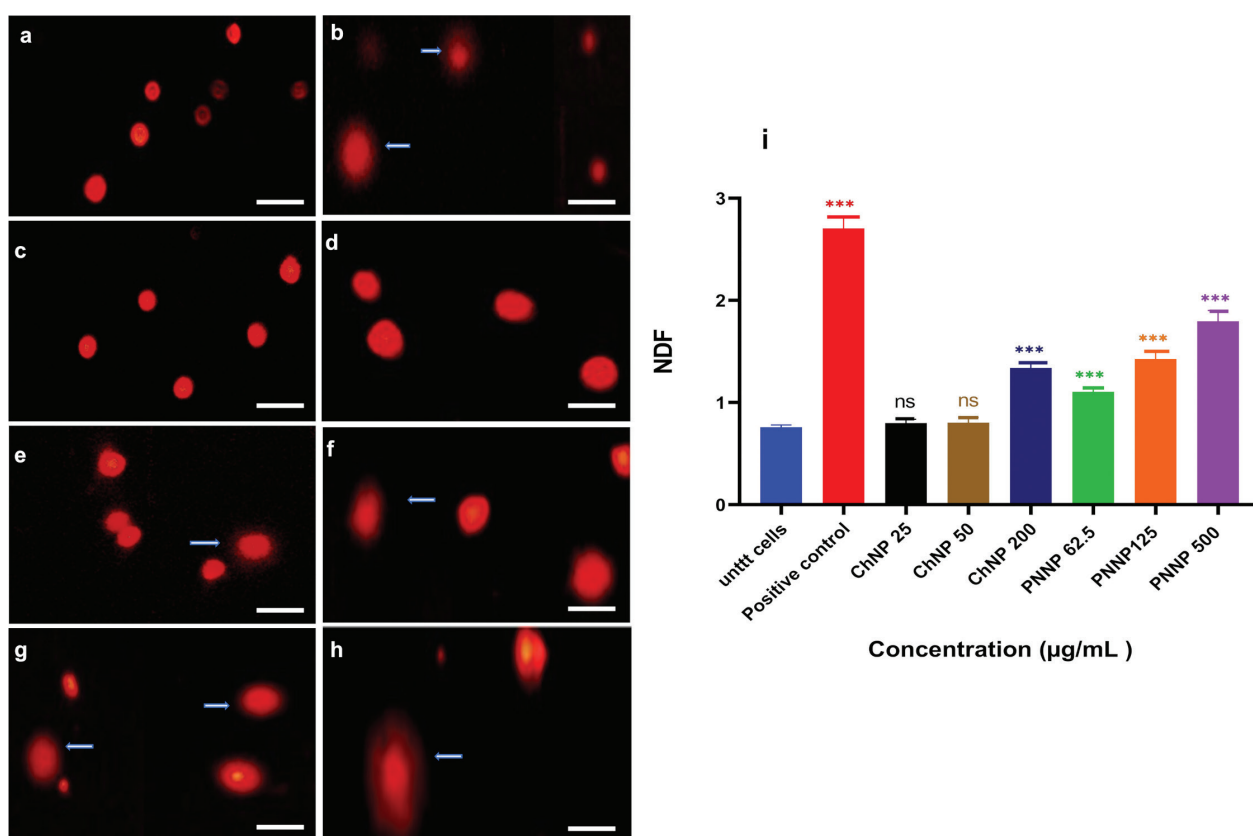


**Figure 6.** DNA breakage caused by ChNP and PNNP using FHA. TM4 cells were incubated with various concentration of ChNP (25, 50, 200  $\mu\text{g}/\text{mL}$ ) and PNNP (62.5, 125, 500  $\mu\text{g}/\text{mL}$ ) for 2 h. Positive control 100  $\mu\text{M}$  H<sub>2</sub>O<sub>2</sub> was used and incubated for 15 min. Photomicrograph obtained by Inverted Microscope Olympus IX73. Single stranded DNA was stained with ethidium bromide of a. NEgative control (untreated cells); b. H<sub>2</sub>O<sub>2</sub>; c. ChNP 25  $\mu\text{g}/\text{mL}$ ; d. ChNP 50  $\mu\text{g}/\text{mL}$ ; e. ChNP 200  $\mu\text{g}/\text{mL}$ ; f. PNNP 62.5  $\mu\text{g}/\text{mL}$ ; g. PNNP 125  $\mu\text{g}/\text{mL}$ ; h. PNNP 500  $\mu\text{g}/\text{mL}$ . The bar indicates 5  $\mu\text{m}$ . i. Histogram showing DNA damage level using NDF from several randomly selected microscope images. The results are shown as mean  $\pm$  SEM of three independent experiments (n=150). ns (not significant) p > 0.05. \*\*\*p < 0.001 when compared to the corresponding control group.

Conversely, incorporation of *Phyllanthus niruri* into the ChNP 25, 50 and 200  $\mu\text{g}/\text{mL}$  (correspond to PNNP 62.5, 125, and 500  $\mu\text{g}/\text{mL}$ , respectively) denoted that halos surrounding the nuclei were gradually enlarged (Fig. 6f–h) and those of the extent of DNA strand scission was significant compared to untreated cells ( $p$ -value  $***p < 0.001$ ), as illustrated in Fig. 6i. The findings in particularly loading *Phyllanthus niruri* into ChNP 20 and 50  $\mu\text{g}/\text{mL}$  suggest that the genotoxic effect of PNNP is predominantly attributable to the *Phyllanthus niruri* extract, as previously demonstrated in the comet assay results. Therefore, caution is warranted when using this extract in nanotechnology applications to ensure safe and effective use.

### Imaging of cellular morphological change by Hoechst 33342 nuclear staining

Hoechst 33342 staining was utilized to determine qualitative changes in cell morphology during apoptosis. The morphological change in nucleus reveals the presence of apoptotic cells which indicated with occurring chromatin condensation and fragmentation of condensed nuclei. As shown in Fig. 7, there was no alterations in cell morpholo-

gy compared to that of untreated cells when it was treated with ChNP 50  $\mu\text{g}/\text{mL}$ . However, in the presence of PNNP 125  $\mu\text{g}/\text{mL}$  and ChNP 200  $\mu\text{g}/\text{mL}$ , fragmented nuclei were observed as indicated by the white arrows. These results indicate that PNNP 125  $\mu\text{g}/\text{mL}$  and ChNP 200  $\mu\text{g}/\text{mL}$  induced apoptosis in TM4 cells. Interestingly, it is likely that the *Phyllanthus niruri* which is the responsible substance to induce the apoptosis since the shell of ChNP 50  $\mu\text{g}/\text{mL}$  did not promote programmed cell death. These results also imply that utilization amount of the carrier ChNP is essential as the increase ChNP concentration from 50 to 200  $\mu\text{g}/\text{mL}$  triggered apoptosis.

### Analysis of BTB proteins expression

Connexin 43 and claudin 11 expression in TM4 cells was determined using an immunofluorescence assay. We used image J software to compute mean fluorescence intensity as a marker for protein expression and analyze protein expression in a semiquantitative manner. Each experiment was repeated twice ( $n = 50$ ), and values are presented as the mean  $\pm$  standard error of the mean (SEM). All data were analyzed using nonparametric one-way ANOVA followed by Kruskal-Wallis for multiple comparisons using

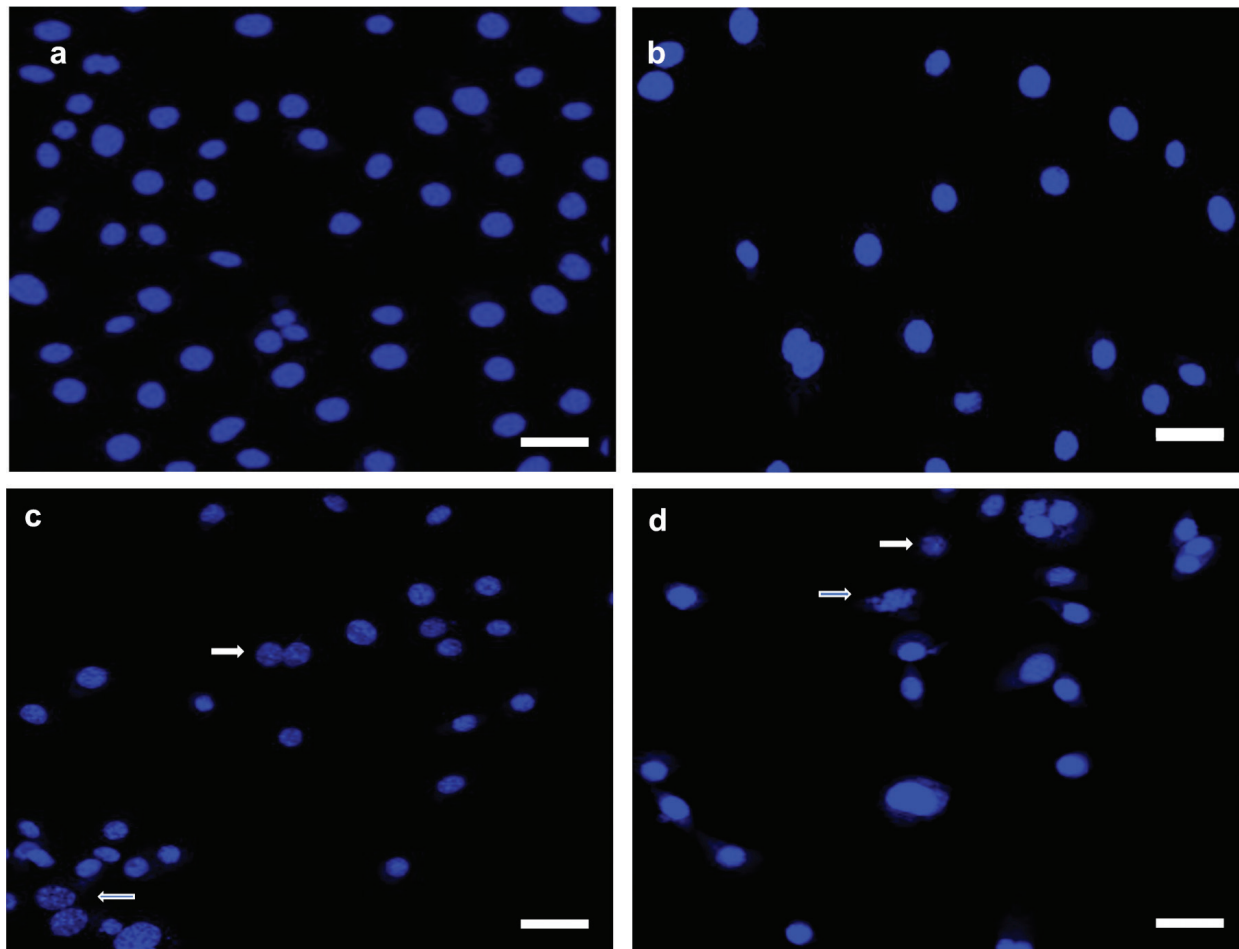


**Figure 7.** Imaging of cellular morphological change in the presence of ChNP and PNNP. TM4 cells were incubated in the absence of nanoparticles (a) and in the presence of ChNP at 50  $\mu\text{g}/\text{mL}$  (b), PNNP at 125  $\mu\text{g}/\text{mL}$  (c), and ChNP at 200  $\mu\text{g}/\text{mL}$  (d). Images were captured 2 h after transfection using a 20 $\times$  lens on a CLSM (Olympus FV-1200) and the nucleus was stained with Hoechst 33342 (blue). The bar indicates 50  $\mu\text{m}$ .

the Graph-Pad Prism 8 software to determine differences in protein expression (mean fluorescence intensity) of treated groups relative to the untreated. Connexin 43 and claudin 11 are two essential junctional proteins. Connexin 43 is vital for mammalian spermatogenesis. Furthermore, multiple studies reveal that connexin 43 is critical for BTB development and BTB homeostasis (Pelletier 1995; Li et al. 2010; Gerber et al. 2016). Claudin 11 is a protein component of the BTB, whose protein expression will be altered if spermatogenesis is stopped or disrupted (Gow et al. 1999). Claudin 11 deficiency could lead to male infertility in mice (Gow et al. 1999; Mazaud-Guittot et al. 2010). As a result, downregulation of connexin 43 and claudin 11 may lead to decreased BTB integrity and spermatogenesis disruption.

After treating TM4 cells with ChNP 200 µg/mL (dilution equivalent to PNNP 500 µg/mL) and PNNP 125 µg/mL for 24 h, there was a significant downregulation of connexin 43 and claudin 11 protein expression with a p-value of  $p < 0.001$  compared to untreated cells, as shown in Figs. 8, 9. In contrast, there was non-significant downregulation of connexin 43 and claudin 11 protein expression in TM4 cells treated with ChNP 50 µg/mL (dilution equivalent to PNNP 125 µg/mL) (Figs 8, 9), with p-values of 0.70 and 0.99, respectively. These results indicate that the non-significant effect of ChNP at this concentration on BTB protein expression in TM4 cells compared to untreated cells. Additionally, treatment of TM4 cells with PNNP 125 µg/mL showed a significant effect on BTB protein expression compared

to ChNP at the same dilution factor. This suggests that the ability to decrease BTB protein expression is mostly from the *Phyllanthus niruri* extract, as confirmed by our previous results indicating that cytotoxicity and genotoxicity effects mainly stem from the *Phyllanthus niruri* extract in nanoscale.

Previous research explained that inorganic silica nanoparticles caused reproductive toxicity by triggering the DNA damage-p53-apoptosis pathway in spermatogenic cells (Liu et al. 2020). Sertoli cells are mesoepithelial somatic cells in the male reproductive system that coordinate and structurally support the growing germ cells. Damage to these cells eventually affects sperm production (Habas et al. 2018). In a separate study, exposure of TM4 cells to sublethal doses of inorganic ZnO nanoparticles caused a significant decrease in BTB protein expression (including claudin-5, occludin, ZO-1, and connexin-43), which led to BTB damage and disruption of spermatogenesis (Liu et al. 2016). The present study found that treatment of TM4 cells with organic PNNP 125 µg/mL and ChNP 200 µg/mL resulted in DNA damage, followed by apoptosis and decreased BTB protein expression. The observed effects could potentially compromise the integrity of the BTB and disrupt the process of spermatogenesis. Furthermore, we have plans to conduct *in vivo* acute and chronic toxicity studies in the future to further investigate the potential toxicity of ChNP and PNNP. These studies will help ensure a comprehensive evaluation of the potential impact of these organic nanoparticles before their use in clinical settings.

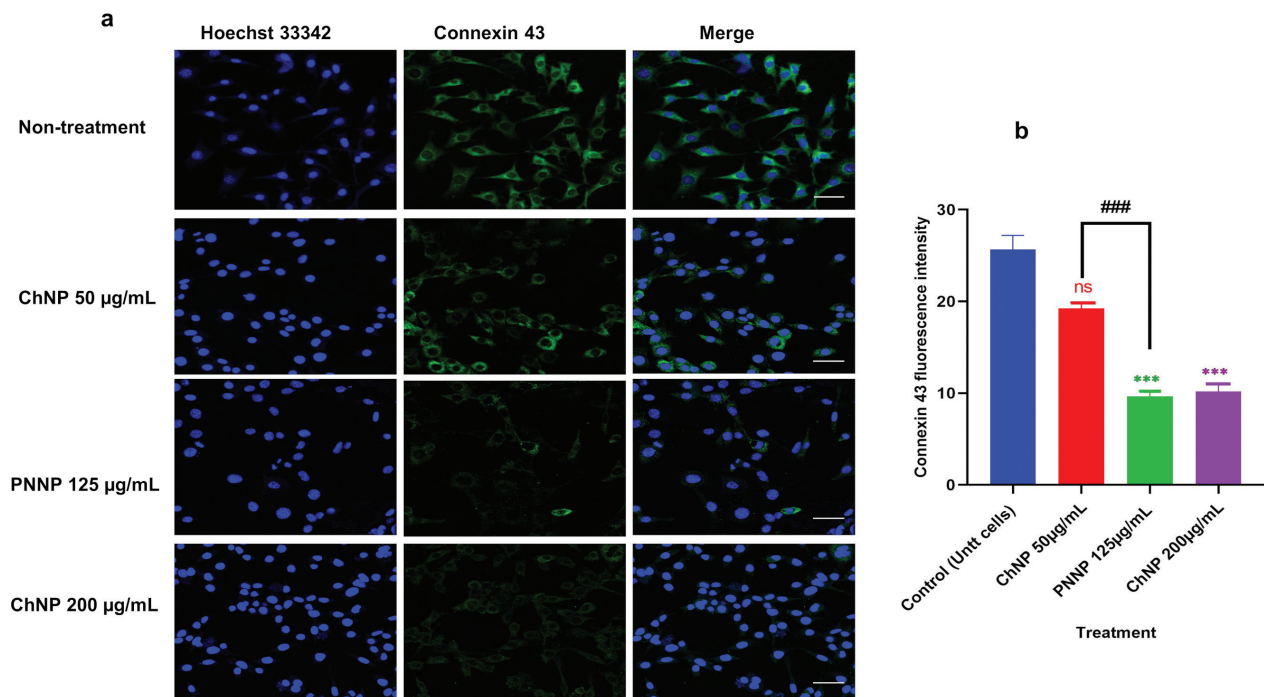


**Figure 8.** Connexin 43 expression in the presence of ChNP and PNNP. TM4 cells were incubated with ChNP 50 µg/mL, PNNP 125 µg/mL and with ChNP 200 µg/mL for 24 h. **a.** Confocal images of connexin 43 expression after cells were incubated with a secondary antibody goat anti-rabbit IgG Alexa Fluor 488 (green) and the nucleus was stained with Hoechst 33342 (blue). The bars indicate 50 µm. **b.** Histogram of downregulation of connexin 43 expression. The results are shown as mean ± SEM of two separate studies (n=50). ns (not significant)  $p > 0.05$ . Stars (\*\*\*) indicate significance when compared with the control group (untreated cells) ( $p < 0.001$ ). Pound signs (###) demonstrate significance compared with ChNP 50 µg/mL.

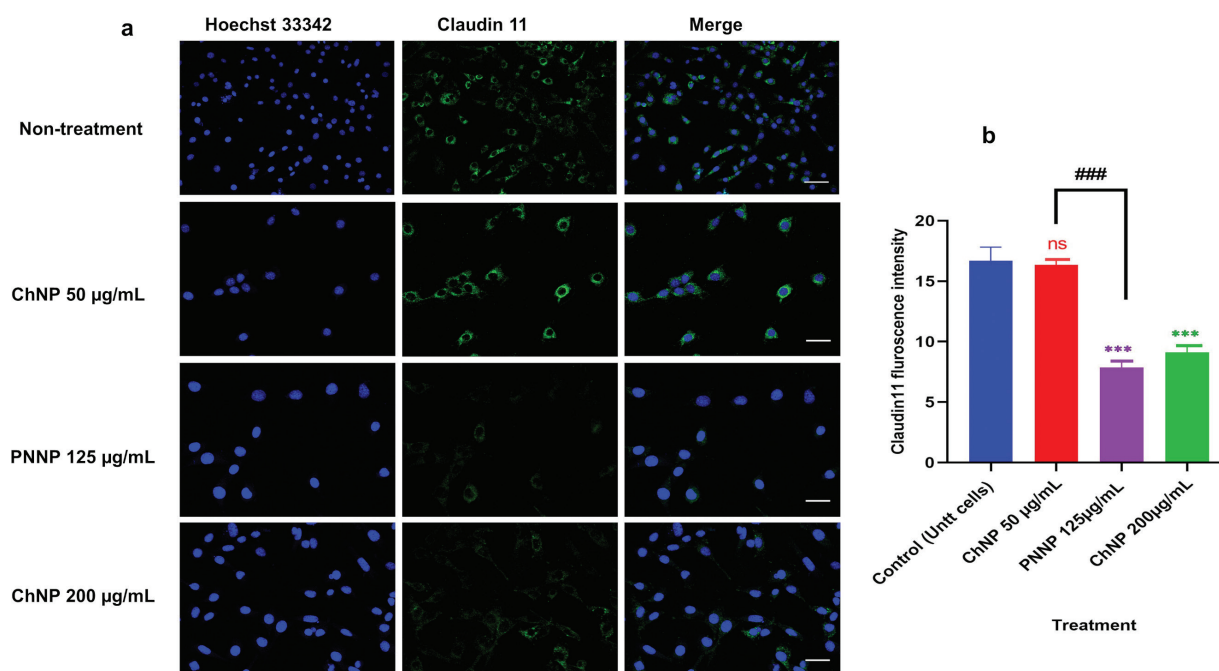


**Figure 9.** Claudin 11 expression in the presence of ChNP and PNNP. TM4 cells were incubated with ChNP 50 µg/mL, PNNP 125 µg/mL and ChNP 200 µg/mL for 24 h. **a.** Confocal images of claudin 11 expression after cells were incubated with a secondary antibody goat anti-rabbit IgG Alexa Fluor 488 (green) and the nucleus was stained with Hoechst 33342 (blue). The bars indicate 50 µm; **b.** Histogram of downregulation claudin 11 expression. The results are shown as mean ± SE of two separate studies (n = 50). ns (not significant)  $p > 0.05$ . Stars (\*\*\*) indicate significance when compared with the control group (untreated cells) ( $p < 0.001$ ). Pound signs (###) demonstrate significance compared with ChNP 50 µg/mL.

## Conclusion

The results of the present study demonstrate that ChNP 25 and 50 µg/mL did not have any cytotoxic or genotoxic effects on TM4 cells, indicating their safety for clinical applications. Although ChNP 200 µg/mL exhibited 94% cell survival, they still caused DNA damage, apoptosis in TM4 cells, and downregulation of BTB proteins, which suggests the potential toxicity of the carrier at the tested concentration. PNNP 62, 125, and 500 µg/mL induced DNA damage, apoptosis in TM4 cells, as well as impaired the integrity of the BTB by downregulating BTB protein expression at PNNP 125 µg/mL, which may contribute to spermatogenesis disruption. The present *Phyllanthus niruri* in ChNP remarkably induced cytotoxic and genotoxic effects on TM4 cell. We emphasize the insufficiency of conventional cytotoxicity assays in ensuring the complete safety of nanoparticles for human use, and strongly advocate for genotoxicity testing of all new nanoparticles before clinical implementation. Overall, the present study underscores the importance of rigorous evaluation of the safety and toxicity of therapeutic cargo and the carrier before their use in human

therapeutics. Our findings provide valuable insights into the potential adverse effects of *Phyllanthus niruri* extract loaded chitosan nanoparticles on male reproductive health.

## Funding

Financial support of this study was mainly provided by the Research, Community Services, and Innovation Program (P3MI), Research Group of ITB (Indonesia).

## Conflict of Interest

The authors declare that they have no conflict of interest.

## Acknowledgments

The authors would like to express their sincere gratitude to the School of Pharmacy, ITB for providing unlimited support towards the research and publication of this article.

## References

- Abou-Saleh H, Younes N, Rasool K, Younis MH, Prieto RM, Yassine HM, Mahmoud KA, Pintus G, Nasrallah GK (2019) Impaired liver size and compromised neurobehavioral activity are elicited by chitosan nanoparticles in the zebrafish embryo model. *Nanomaterials* 9(1): 122. <https://doi.org/10.3390/nano9010122>
- Allen S, Sotos J, Sylte MJ, Czuprynski CJ (2001) Use of hoechst 33342 staining to detect apoptotic changes in bovine mononuclear phagocytes infected with *Mycobacterium avium* subsp. *paratuberculosis*. *Clinical and Diagnostic Laboratory Immunology* 8(2): 460–464. <https://doi.org/10.1128/CDLI.8.2.460-464.2001>

- Asare GA, Bugyei K, Fiawoyi I, Asiedu-Gyekye IJ, Gyan B, Adjei S, Addo P, Otu-Nyarko L, Nyarko A (2013) Male rat hormone imbalance, testicular changes and toxicity associated with aqueous leaf extract of an antimalarial plant: *Phyllanthus niruri*. *Pharmaceutical Biology* 51(6): 691–699. <https://doi.org/10.3109/13880209.2013.764325>
- Bagalkotkar G, Sagineedu SR, Saad MS, Stanslas J (2010) Phytochemicals from *Phyllanthus niruri* Linn. and their pharmacological properties: a review. *Journal of Pharmacy and Pharmacology* 58(12): 1559–1570. <https://doi.org/10.1211/jpp.58.12.0001>
- Daramola OE, Adelaja OA (2020) Preparation of chitosan nanoparticles from crab shell and their characterization. *International Journal of Materials Chemistry and Physics* 6.
- Dash M, Chiellini F, Ottenbrite RM, Chiellini E (2011) Chitosan - A versatile semi-synthetic polymer in biomedical applications. *Progress in Polymer Science (Oxford)* 36(8): 981–1014. <https://doi.org/10.1016/j.progpolymsci.2011.02.001>
- De Melo MN, Lira Soares LA, Da Costa Porto CR, De Araújo AA, Das Graças Almeida M, De Souza TP, Petrovick PR, De Araújo Júnior RF, Guerra GCB (2015) Spray-dried extract of *Phyllanthus niruri* L. reduces mucosal damage in rats with intestinal inflammation. *Journal of Pharmacy and Pharmacology* 67(8): 1107–1118. <https://doi.org/10.1111/jphp.12408>
- Dusinska M, Rundén-Pran E, El Yamani N, Fjellsbø LM, Collins A (2017) Chapter 17: Application of the Comet Assay in Nanotoxicology. In: Anderson D, Dhawan A (Eds) *The Comet Issues in Toxicology*, 477–497. <https://doi.org/10.1039/9781782622895-00477>
- Ezzat MI, Okba MM, Ahmed SH, El-Banna HA, Prince A, Mohamed SO, Ezzat SM (2020) In-depth hepatoprotective mechanistic study of *Phyllanthus niruri*: *In vitro* and *in vivo* studies and its chemical characterization. *PLoS ONE* 15(1): e0226185. <https://doi.org/10.1371/journal.pone.0226185>
- Freitas AM, Schor N, Boim MA (2002) The effect of *Phyllanthus niruri* on urinary inhibitors of calcium oxalate crystallization and other factors associated with renal stone formation. *BJU International* 89(9): 829–834. <https://doi.org/10.1046/j.1464-410X.2002.02794.x>
- Frigaard J, Jensen JL, Galtung HK, Hiorth M (2022) The potential of chitosan in nanomedicine: An overview of the cytotoxicity of chitosan based nanoparticles. *Frontiers in Pharmacology* 13. <https://doi.org/10.3389/fphar.2022.880377>
- Gerber J, Heinrich J, Brehm R (2016) Blood-testis barrier and Sertoli cell function: Lessons from SCCx43KO mice. *Reproduction* 151(2): R15–R27. <https://doi.org/10.1530/REP-15-0366>
- Giribabu N, Karim K, Kilari EK, Salleh N (2017) *Phyllanthus niruri* leaves aqueous extract improves kidney functions, ameliorates kidney oxidative stress, inflammation, fibrosis and apoptosis and enhances kidney cell proliferation in adult male rats with diabetes mellitus. *Journal of Ethnopharmacology* 205: 123–137. <https://doi.org/10.1016/j.jep.2017.05.002>
- Gow A, Southwood CM, Li JS, Pariali M, Riordan GP, Brodie SE, Danias J, Bronstein JM, Kachar B, Lazzarini RA (1999) CNS Myelin and sertoli cell tight junction strands are absent in OSP/claudin-11 null mice. *Cell* 99(6): 649–659. [https://doi.org/10.1016/S0092-8674\(00\)815536](https://doi.org/10.1016/S0092-8674(00)815536)
- Habas K, Brinkworth MH, Anderson D (2018) Silver nanoparticle-mediated cellular responses in isolated primary Sertoli cells *in vitro*. *Food and Chemical Toxicology* 116: 182–188. <https://doi.org/10.1016/j.fct.2018.04.030>
- Hidanah S, Sabdoningrum EK, Sudjarwo SA (2022) Formulation and characterization of meniran (*Phyllanthus niruri* Linn) extract nanoparticle on antibacterial activity against *Salmonella pullorum*. *Pharmacognosy Journal* 14(2): 369–373. <https://doi.org/10.5530/pj.2022.14.47>
- Hu YL, Gao JQ (2010) Potential neurotoxicity of nanoparticles. *International Journal of Pharmaceutics* 394: 115–121. <https://doi.org/10.1016/j.ijpharm.2010.04.026>
- Hu YL, Qi W, Han F, Shao JZ, Gao JQ (2011) Toxicity evaluation of biodegradable chitosan nanoparticles using a zebrafish embryo model. *International journal of nanomedicine* 6: 3351–3359. <https://doi.org/10.2147/ijn.s25853>
- Kahdestani SA, Shahriari MH, Abdouss M (2021) Synthesis and characterization of chitosan nanoparticles containing teicoplanin using sol-gel. *Polymer Bulletin* 78: 1133–1148. <https://doi.org/10.1007/s00289-020-03134-2>
- Kaur N, Kaur B, Sirhindi G (2017) Phytochemistry and pharmacology of *Phyllanthus niruri* L.: A Review. *Phytotherapy Research* 31(7): 980–1004. <https://doi.org/10.1002/ptr.5825>
- Kemenkes ARI (2017) *Farmakope herbal indonesia edisi II*. Jakarta: Kemenkes RI.
- Lewinski N, Colvin V, Drezek R (2008) Cytotoxicity of nanoparticles. *Small* 4(1): 26–49. <https://doi.org/10.1002/sml.200700595>
- Li MWM, Mruk DD, Lee WM, Cheng CY (2010) Connexin 43 is critical to maintain the homeostasis of the blood-testis barrier via its effects on tight junction reassembly. *Proceedings of the National Academy of Sciences of the United States of America* 107(42): 17998–18003. <https://doi.org/10.1073/pnas.1007047107>
- Liu J, Li X, Zhou G, Sang Y, Zhang Y, Zhao Y, Ge W, Sun Z, Zhou X (2020) Silica nanoparticles induce spermatogenesis disorders via L3MBTL2-DNA damage-p53 apoptosis and RNF8-ubH2A/ubH2B pathway in mice. *Environmental Pollution* 265: 14974. <https://doi.org/10.1016/j.envpol.2020.114974>
- Liu Q, Xu C, Ji G, Liu H, Mo Y, Tollerud DJ, Gu A, Zhang Q (2016) Sublethal effects of zinc oxide nanoparticles on male reproductive cells. *Toxicology in Vitro* 35: 131–138. <https://doi.org/10.1016/j.tiv.2016.05.017>
- Loh JW, Yeoh G, Saunders M, Lim LY (2010) Uptake and cytotoxicity of chitosan nanoparticles in human liver cells. *Toxicology and Applied Pharmacology* 249(2): 148–157. <https://doi.org/10.1016/j.taap.2010.08.029>
- Mahmood MA, Madni A, Rehman M, Rahim MA, Jabar A (2019) Ionically cross-linked chitosan nanoparticles for sustained delivery of docetaxel: Fabrication, post-formulation and acute oral toxicity evaluation. *International Journal of Nanomedicine* 14: 10035–10046. <https://doi.org/10.2147/IJN.S232350>
- Maurya DK (2014) HaloJ: An imageJ program for semiautomatic quantification of DNA damage at single-cell level. *International Journal of Toxicology* 33(5): 362–366. <https://doi.org/10.1177/1091581814549961>
- Mazaud-Guittot S, Meugnier E, Pesenti S, Wu X, Vidal H, Gow A, Le Mageresse-Battistoni B (2010) Claudin 11 deficiency in mice results in loss of the sertoli cell epithelial phenotype in the testis. *Biology of Reproduction* 82(1): 202–213. <https://doi.org/10.1095/biolreprod.109.078907>
- Mohamed AA, Kbah NZ, Wennas ON (2023) Poly (lactic-co-glycolic acid) nanoparticles for drug delivery of rupatadine fumarate: development and evaluation. *Pharmacia* 70(4): 1257–1264. <https://doi.org/10.3897/pharmacia.70.e110191>
- Moseson DE, Jordan MA, Shah DD, Corum ID, Alvarenga BR, Taylor LS (2020) Application and limitations of thermogravimetric analysis to delineate the hot melt extrusion chemical stability processing win-

- dow. International Journal of Pharmaceutics 590: 119916. <https://doi.org/10.1016/j.ijpharm.2020.119916>
- Nagai H, Okazaki Y, Chew SH, Misawa N, Yamashita Y, Akatsuka S, Ishihara T, Yamashita K, Yoshikawa Y, Yasui H, Jiang L, Ohara H, Takahashi T, Ichihara G, Kostarelou K, Miyata Y, Shinohara H, Toyokuni S (2011) Diameter and rigidity of multiwalled carbon nanotubes are critical factors in mesothelial injury and carcinogenesis. Proceedings of the National Academy of Sciences of the United States of America 108(49): E1330–E1338. <https://doi.org/10.1073/pnas.1110013108>
- Nandanpawar PC, Ashraf Rather M, Ramesh Badhe M, Sharma R (2018) Assessment of DNA Damage During Gene Delivery in Freshwater Prawn by Chitosan Reduced Gold Nanoparticles. Biosciences, Biotechnology Research Asia 15: 1. <https://doi.org/10.13005/bbra/2606>
- Pathania R, Najda A, Chawla P, Kaushik R, Khan MA (2022) Low-energy assisted sodium alginate stabilized *Phyllanthus niruri* extract nanoemulsion: Characterization, *in vitro* antioxidant and antimicrobial application. Biotechnology Reports 33: e00711. <https://doi.org/10.1016/j.btre.2022.e00711>
- Pelletier R-M (1995) The distribution of Connexin 43 is associated with the germ cell differentiation and with the modulation of the Sertoli cell junctional barrier in continual (Guinea pig) and seasonal breeders' (Mink) testes. Journal of Andrology 16(5): 400–409. <https://doi.org/10.1002/j.1939-4640.1995.tb00552.x>
- Pratiwi G, Martien R, Murwanti R (2019) Chitosan nanoparticle as a delivery system for polyphenols from meniran extract (*Phyllanthus niruri* L.): Formulation, optimization, and immunomodulatory activity. International Journal of Applied Pharmaceutics 11(2): 50–58. <https://doi.org/10.22159/ijap.2019v11i2.29999>
- Puzyn T, Rasulev B, Gajewicz A, Hu X, Dasari TP, Michalkova A, Hwang HM, Toropov A, Leszczynska D, Leszczynski J (2011) Using nano-QSAR to predict the cytotoxicity of metal oxide nanoparticles. Nature Nanotechnology 6: 175–178. <https://doi.org/10.1038/nano.2011.10>
- Ramos P, Raczak BK, Silvestri D, Wacławek S (2023) Application of TGA/c-DTA for distinguishing between two forms of naproxen in pharmaceutical preparations. Pharmaceutics 15(6): 1689. <https://doi.org/10.3390/pharmaceutics15061689>
- Rizeq BR, Younes NN, Rasool K, Nasrallah GK (2019) Synthesis, bioapplications, and toxicity evaluation of chitosan-based nanoparticles. International Journal of Molecular Sciences 20(22): 5776. <https://doi.org/10.3390/ijms20225776>
- Schmid I, Uittenbogaart C, Jamieson BD (2007) Live-cell assay for detection of apoptosis by dual-laser flow cytometry using Hoechst 33342 and 7-amino-actinomycin D. Nature Protocols 2: 187–190. <https://doi.org/10.1038/nprot.2006.458>
- Sestili P, Martinelli C, Stocchi V (2006) The fast halo assay: An improved method to quantify genomic DNA strand breakage at the single-cell level. Mutation Research - Genetic Toxicology and Environmental Mutagenesis 607(2): 205–214. <https://doi.org/10.1016/j.mrgentox.2006.04.018>
- Sricharoenchaikul V, Atong D (2009) Thermal decomposition study on *Jatropha curcas* L. waste using TGA and fixed bed reactor. Journal of Analytical and Applied Pyrolysis 85: 155–162. <https://doi.org/10.1016/j.jaap.2008.11.030>
- Tice RR, Agurell E, Anderson D, Burlinson B, Hartmann A, Kobayashi H, Miyamae Y, Rojas E, Ryu JC, Sasaki YF (2000) Single cell gel/comet assay: Guidelines for *in vitro* and *in vivo* genetic toxicology testing. Environmental and Molecular Mutagenesis 35(3): 206–221. [https://doi.org/10.1002/\(SICI\)1098-2280\(2000\)35:3<206::AID-EM8>3.0.CO;2-J](https://doi.org/10.1002/(SICI)1098-2280(2000)35:3<206::AID-EM8>3.0.CO;2-J)
- Unni RT, Shah GA, Snima KS, Kamath CR, Nair S V., Lakshmanan VK (2014) Enhanced delivery of *Phyllanthus niruri* nanoparticles or prostate cancer therapy. Journal of Bionanoscience 8(2): 101–107. <https://doi.org/10.1166/jbns.2014.1204>
- Vaezifar S, Razavi S, Golozar MA, Karbasi S, Morshed M, Kamali M (2013) Effects of some parameters on particle size distribution of chitosan nanoparticles prepared by ionic gelation method. Journal of Cluster Science 24: 891–903. <https://doi.org/10.1007/s10876-013-0583-2>
- Wang Y, Zhou J, Liu L, Huang C, Zhou D, Fu L (2016) Characterization and toxicology evaluation of chitosan nanoparticles on the embryonic development of zebrafish, *Danio rerio*. Carbohydrate Polymers 141: 204–210. <https://doi.org/10.1016/j.carbpol.2016.01.012>
- Wu JH, Jones NJ (2012) Assessment of DNA interstrand crosslinks using the modified alkaline comet assay. Methods in Molecular Biology 817: 165–181. [https://doi.org/10.1007/978-1-61779-421-6\\_9](https://doi.org/10.1007/978-1-61779-421-6_9)
- Yang H, Du L, Tian X, Fan Z, Sun C, Liu Y, Keelan JA, Nie G (2014) Effects of nanoparticle size and gestational age on maternal biodistribution and toxicity of gold nanoparticles in pregnant mice. Toxicology Letters 230(1): 10–18. <https://doi.org/10.1016/j.toxlet.2014.07.030>

## Supplementary material 1

### Supplementary information

Authors: Ebrahim Sadaqa, Ratna Annisa Utami, Diky Mudhakir  
Data type: docx

Copyright notice: This dataset is made available under the Open Database License (<http://opendatacommons.org/licenses/odbl/1.0>). The Open Database License (ODbL) is a license agreement intended to allow users to freely share, modify, and use this Dataset while maintaining this same freedom for others, provided that the original source and author(s) are credited.

Link: <https://doi.org/10.3897/pharmacia.71.e112138.suppl1>